INVESTIGATION OF THE MULTI-SCALE INTERACTIONS BETWEEN AN OFFSHORE WIND TURBINE WAKE AND THE OCEAN-SEDIMENT DYNAMICS IN A INDEALIZED FRAMEWORK

Tim Nagel, Julien Chauchat, Achim Wirth

E-proceedings of the 36th IAHR World Congress,
28 June - 3 July, 2015, The Hague, the Netherlands

INVESTIGATION OF THE MULTI-SCALE INTERACTIONS BETWEEN AN OFFSHORE WIND TURBINE WAKE AND THE OCEAN-SEDIMENT DYNAMICS IN A INDEALIZED FRAMEWORK

Tim Nagel[1], Julien Chauchat[2], Achim Wirth[3]

[1] LEGI Domaine Universitaire, BP 53, 38041 Grenoble Cedex 9, France.
Tim.Nagel@grenoble-inp.fr
[2] LEGI Domaine Universitaire, BP 53, 38041 Grenoble Cedex 9, France.
Julien.Chauchat@grenoble-inp.fr
[3] LEGI Domaine Universitaire, BP 53, 38041 Grenoble Cedex 9, France.
Achim.Wirth@legi.cnrs.fr

ABSTRACT

A coupled two dimensional idealized numerical model of the ocean and sediment layers, forced by an offshore wind turbine wake is used to investigate the complex interactions between the wake, the ocean and the sediment layers, together with the retro-action on the wind energy. Results show that the turbine wake has an impact on both, the ocean and the sediment layers. The turbine wake impacts the ocean surface and generates instabilities or vortex streets for some parameter values. Shallow ocean layers (typically below 15m) are laminar. When water depth is higher, large scale instabilities are generated, leading to a turbulent dynamic in the ocean layer. The size of the generated vortices in the ocean increases with water depth and decreases with the quadratic-law bottom friction coefficient. Considering the morphodynamics three cases are observed, depending on whether the ocean dynamics is laminar (i), has a localized (ii) or domain wide (iii) turbulent behavior. In the first case, changes in seabed elevation are around a few millimeters per month. Results are similar for the localized turbulence case with small spatial variations. For the domain wide turbulence case (iii), instantaneous seabed changes are of the order of a few millimeters per month, whereas the transport averaged over several days decreases to a few tenths of millimeter per month. This behavior is easily explained by the oscillating local velocity which transports sediments back and forth. The above emphasizes that the water depth is a key parameter for the coupled atmosphere-ocean-sediment system around wind turbines. Furthermore, considering the ocean velocity in the atmospheric forcing at the ocean surface leads to a decrease of 4 $\%$ of the power lost by friction at the atmosphere-ocean interface. Ocean dynamics could thus have a non-negligible feedback on the wind power available for the turbines and its variability.

Key words: Offshore Wind Turbine; Wake; Ocean; Seabed; Dynamics.

1. INTRODUCTION

Because of the rising need for sustainable energy, and because up to now wind energy is one of the few forms of renewable energy that can be harvested efficiently, many European countries are planning and building offshore wind farms to increase the proportion of renewable energy in their energy mix. According to the European Wind Energy Association 2013 annual report (*EWEA*, 2013), the installed European capacity was 5 GW at the end of 2012, and by 2020 it could be multiplied by 8 (40 GW), corresponding to 4$\%$ of the European electricity demand. By 2030, offshore wind capacity could totalize 150 GW, corresponding to 14$\%$ of the actual EU's total electricity consumption.

The environmental impact of wind farm construction is the subject of an important and diversified literature. A consequent part of this literature focus on the direct impacts of the solid structures of the wind farm on the oceanic environment and principaly on the fauna. An important environmental consequence is the birds and bats collision with the turbines (*Tucker* (1996), *Drewitt and Langston* (2006)). Concerning the seabed, it is affected by scour process due to the pile presence, a phenomenon similar to that of occurs at bridge piers (*Breusers et al.* (1977), *Breusers and Raudkivi* (1991), *Roulund et al.* (2005)). It has also been shown that a local seabed elevation occurs in offshore wind farms (*Van der Veen et al.*, 2007). On a larger scale, impact of wind farms on the European regional climate (*Vautard et al.*, 2014) or on hurricanes (*Jacobson et al.*, 2014) have been studied recently, showing that the wind farms environmental impacts are an important questions nowadays.

Nevertheless, most of the interactions between offshore wind farms and their local environment need further research and the understanding of the global impact induced by the construction of offshore wind farms in coastals areas may requires the modeling of the ocean-atmosphere-sediment coupled system. However, if air-sea and ocean-sediment interactions have been the subject of an important literature, to the best of our knowledge, no study has been done on the multi-scale interactions in an atmosphere-ocean-sediment coupled system. This is even more true in the vicinity of Marine Renewable Energy Devices.
This paper shows the first results of an idealized 2D numerical model build to study the impact of an offshore turbine wake on the

ocean and the sediment dynamics. In Section 2., the physical model and the basic equations that describe the mathematical model are detailled. The numerical model used here is described in Section 3., while Section 4. is devoted to the presentation and the discussion of the results. The summary and conclusions are given in Section 5.

2. PHYSICAL AND MATHEMATICAL MODEL

The physical model consists in two superposed layers (figure 1.a), an homogeneous shallow water ocean layer above a sediment bed layer, composed of cohesion-less particles. The atmospheric layer is represented as an external forcing (F), which corresponds to the wake of wind turbines. The domain length in the x-direction is denoted as L_x and as L_y in the y-direction. The average depth

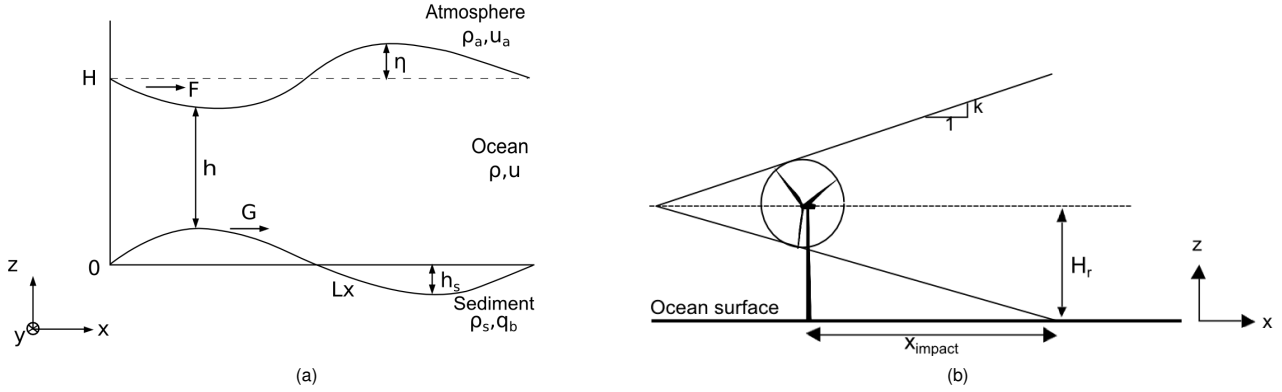

Figure 1: Sketch of the physical model, exponent "s" refers to the sediment bed (a) and of the Jensen wake (b).

of the ocean layer is denoted as H. The local thickness of the ocean layer and the seabed elevation, are denoted as $h(x, y, t)$ and $h_s(x, y, t)$ respectively. The free surface elevation is:

$$\eta(x, y, t) = h(x, y, t) - H + h_s(x, y, t) \quad [1]$$

The dimensional variables are consigned in the table 1. Densities are denoted as ρ, ρ_s and ρ_a for the ocean, the sediment and the atmosphere, respectively, D_s is the diameter of a sand grain. The ocean layer is forced by the local wind stress at its upper surface. The spatial variation of this wind stress incorporates the wake-profile of a wind turbine. The oceanic motion induces a shear stress

Table 1: Domain parameters.

ρ (kg.m^{-3})	ρ_s (kg.m^{-3})	ρ_a (kg.m^{-3})	L_x (m)	L_y (m)	H (m)	D_s (m)
1025	2650	1.2	10^3	10^3	10-50	2^{-4}

τ_b on the sediment bed layer. This stress and the seabed elevation are responsible for the coupling between the ocean and the sediment bed layers.

2.1 Hydrodynamic model

Mathematically, the ocean dynamic is given by the two dimensional Shallow Water (SW) equations, as most of the wind farms are localized in coastal areas (in 2012 the average water depth of offshore wind farms was 22m and the average distance to shore was 29km (*EWEA*, 2013)), such equations seem to be particularly adapted to the problem:

$$\partial_t \overrightarrow{u} + (\overrightarrow{u} \cdot \nabla)\overrightarrow{u} + g\nabla\eta \; = \; \nu\nabla^2\overrightarrow{u} + \overrightarrow{F} - \overrightarrow{G} \quad [2]$$

$$\partial_t h + \nabla(h\overrightarrow{u}) \; = \; 0, \quad [3]$$

where $\overrightarrow{F}$ and $\overrightarrow{G}$ correspond to the frictionnal accelerations applied on the ocean layer by the atmosphere and the sediment, respectively. These frictionnal accelerations correspond to the forces excerted on the ocean by the wind shear and the bottom shear respectively and are characterized by a quadratic friction law. The atmosphere$-$ocean friction law ($\overrightarrow{F}$) is defined by:

$$\overrightarrow{F} = \frac{1}{\rho h}\,\overrightarrow{f}, \quad [4]$$

where $\overrightarrow{f}$ is the shear stress applied to the ocean. The latter is calculated using the velocity difference between wind and ocean current as described by *Moulin and Wirth* (2014):

$$\overrightarrow{f} = C_D\,\rho_a \,||\, \overrightarrow{u}_a - \overrightarrow{u}_o \,||\, (\overrightarrow{u}_a - \overrightarrow{u}_o) \quad [5]$$

with $|| \overrightarrow{u}_a - \overrightarrow{u}_o || = \sqrt{(u_a - u_o)^2 + (v_a - v_o)^2}$. The drag coefficient C_D follows *Wu* (1982) and *Smith* (1988) suggestion:

$$C_D = (0.6 + 0.07u).10^{-3} \quad \text{for } 6 \text{ m/s} < \text{u}_\text{a} < 26 \text{ m/s} \tag{6}$$

The validity range of this friction law corresponds to the good working conditions of wind turbines (from 4 m.s^{-1} to 25 m.s^{-1}). A similar quadratic friction law is used to model the friction between the ocean and the sediment layers:

$$\overrightarrow{G} = \frac{1}{h} \overrightarrow{\tau_b}, \tag{7}$$

$$\overrightarrow{\tau_b} = C_{Ds} \; || \overrightarrow{u} || \overrightarrow{u}, \tag{8}$$

with $|| \overrightarrow{u} || = \sqrt{u^2 + v^2}$. $C_{Ds} = 0.005$ correspond to the friction coefficient between the sand and the ocean.

2.2 Morphodynamic model

For a bed composed of cohesionless grains (equivalent to sand), the sediment starts to move when the drag force exerted by the flow is higher than the friction force between the grains. The dimensionless Shields parameter (*Shields*, 1936), gives the ratio between the drag force and the apparent submerged grains weight:

$$\theta = \frac{\tau_b}{(\rho_s - \rho) g d}, \tag{9}$$

where g is the gravitational acceleration and d is the characteristic sediment particle diameter.
The sediment starts to move as soon as the Shields parameter exceeds a typical critical value ($\theta > \theta_c$). The critical Shields parameter, θ_c gives the threshold of motion for sediments at the bed and depends on several sediment properties, as the density or the grain size.
Bed motion results from a local flux balance. The mass conservation equation, also called Exner equation, allows to calculate the time evolution of the seabed elevation (h_s):

$$\partial_t h_s(x, y, t) + \overrightarrow{\nabla} \cdot \overrightarrow{q}(x, y, t) = 0, \tag{10}$$

where $\overrightarrow{q}$ is the total sediment flux.
Two modes of sediment transport exists, bed-load transport and suspended load transport. In this work, only the bed-load transport will be considered, this type of transport is generally dominating for rather low bed shear stress, i.e when the Shields number of the flow is juste above the critical value.
If only bed-load transport is considered, the total sediment flux becomes:

$$\overrightarrow{q} = \frac{1}{1 - p} \overrightarrow{q}_b, \tag{11}$$

where p is the bed porosity and $\overrightarrow{q}_b$ is the bed load transport rate.
In the present model, the *Meyer-Peter and Müller* (1948) (MPM) transport formula is used. It relates the particle flux q_b to the excess Shields parameter:

$$\frac{q_b}{d\sqrt{(\rho_s/\rho) g d}} = \begin{cases} 8(\theta - \theta_c)^{3/2} & \text{if } \theta > \theta_c \\ 0 & \text{otherwise} \end{cases} \tag{12}$$

2.3 Turbine wake model

According to *Barbe* (2013), the turbine wake affects the ocean by decreasing the surface shear in the region where the wake intersects the ocean surface (see figure 1). This perturbation is maximal at the impact location and then decreases downstream. A distance of 40 to 60 times the rotor diameter D is necessary for the wake effects to vanish.
The wake model used in this work describes the velocity deficit induced by the rotor in the far wake region. The simplest model is the *Jensen* (1983) one, assuming a linearly expanding or cone wake with a velocity deficit which only depends of the distance to the rotor.

$$u = U_\infty \left[1 - \frac{1 - \sqrt{1 - C_w}}{(1 + \frac{2kx}{D})^2} \right], \tag{13}$$

where U_∞ is the wind velocity far from the turbine, C_w the drag coefficient between the turbine and the air and k the Wake Decay Constant. For offshore turbines, the admitted value is equal to 0.05.

The wake impacts the ocean surface at a given distance downstream from the rotor position (figure 1.b). For the Jensen's model we have:

$$x_{impact} = \frac{H_r - D/2}{k} \tag{14}$$

This impact distance depends on the wind turbine height and on the rotor diameter and is increasing with the turbine size. For the turbines considered here ($H_r = 70$m and $D = 80$m, $k = 0.05$), the impact distance is equal to 600 meters, several times the

turbine height. Perturbations in the seabed induced by the turbine pile are localized in the pile vicinity, the seabed is thus perturbed on a local scale. As the pile diameter doesn't exceed 5 meters for the type of turbine modeled, seabed perturbations induced by the pile and the wake presence are uncorrelated. The effect of the pile is thus not considered here.

The Jensen wake model's boundaries are extremely sharp, indeed, the velocity difference between inside and outside the wake corresponds to a step function. Such sharp boundaries are unrealistic and are prone to generating instabilities. To be more realistic without changing the large scale characteristic of the wake model, a good solution consists in using a mollifier (also known as approximation to the identity) function. Thus, close to the wake boundary, the wind velocity u_a is smoothed and becomes $\widetilde{u_a}$ by using the following operator:

$$\widetilde{u_a}(y) = \frac{1}{L_m\sqrt{\pi}} \int_a^b u_a(y') e^{-\left(\frac{y-y'}{L_m}\right)^2} dy', \qquad [15]$$

where $a = L_y/2$ and $b = L_y$ or $b = 1$ are the integral bounds, for the upper and the lower wake boundaries, respectively, $y' = y'(x)$ is the position of the wake boundary and $L_m \approx 1 - 10\ dy$ is the mollify length, for $L_m = 1$, the transition zone correspond to a step function.

3. NUMERICAL MODEL

The ocean and the sediment are considered in a rectangle of size $L_x \times L_y$. The numerical grid is regular and contains $n_x \times n_y$ points. The number of grid points is equal to the length (in meters) of the domain in each direction, $i.e\ L_x = 2000$m and $L_y = 600$m. The spatial resolution is the same in both horizontal directions, $\Delta x = L_x/n_x = \Delta y = L_y/n_y = 1$ m. Periodic boundary conditions are used in both horizontal directions.
The overall model can be divided in two coupled modules, the hydrodynamic and the morphodynamic ones. Concerning the hydrodynamic module, where the shallow water equations for the ocean are solved, a second-order, centered, finite-difference method is used for the space discretization, and a second-order Runge−Kutta scheme is used for the time discretization. The morphodynamic module solves the Exner equation using a NOCS (Non−Oscillatory Central Scheme) scheme as described by *Jiang et al.* (1998).
For a given spatial resolution, the time step is imposed by the Courant−Friedrichs−Lewy (CFL) condition. The sand waves propagation celerity corresponds to dunes migration speed which is approximatively 1000 times slower than oceanic waves. It is thus the CFL condition for the ocean that sets the maximum time step, here $\Delta t = 0.02$ s. As the morphological timescale is large compared to the hydrodynamic one, two time-steps are used, the morphological the time-step is $\Delta t_{morpho} = 1000\ \Delta t$ for all the simulations.

4. RESULTS AND DISCUSSIONS

All the numerical simulations presented in this work involve the same wake parameters, such as the rotor diameter or the wind velocity. The rotor diameter and height ($D = 80$m, $H_r = 70$m) correspond to a Vestas V80−2.0 MW wind turbine, one of the most widespread offshore wind turbines. The wind speed is equal to 20m.s^{-1}, corresponding to the high range part of turbine good working conditions (from 4m.s^{-1} to 25m.s^{-1}) [1]. Simulations have been undertaken for five different water depths and a summary of the different simulations parameters is given in table 2. Run H20CD2P3 has been undertaken with a bottom friction coefficient $C_{Ds'} = (2/3) * C_{Ds}$, run H15WUo without the ocean velocity in the calculations of the atmospheric forcing, run H30WUow without the wake and the ocean velocity in the calculations of the atmospheric forcing and run H30Ww without including the wake in the calculations of the atmospheric forcing. So in run H30WUow and H30Ww the forcing is constant in time and space and the solutions in the ocean and sediment converge to a stationary state (and can be calculated analytically). For each case, the initial free surface and seabed elevation fields are equal to zero.

Table 2: Wake simulations and their parameters.

Run name	H (m)	Eddies Diameter (D_e (m))	Eddies spacing (L_e (m))
H15	15	-	-
H20	20	100	400
H30	30	250	500
H40	40	300-400	670
H50	50	550	1000
H20CD2P3	20	250	500
H15WUo	15	-	-
H30WUow	30	-	-
H30Ww	30	-	-

[1] Vestas V80-2.0 MW product brochure: *http://www.vestas.com*

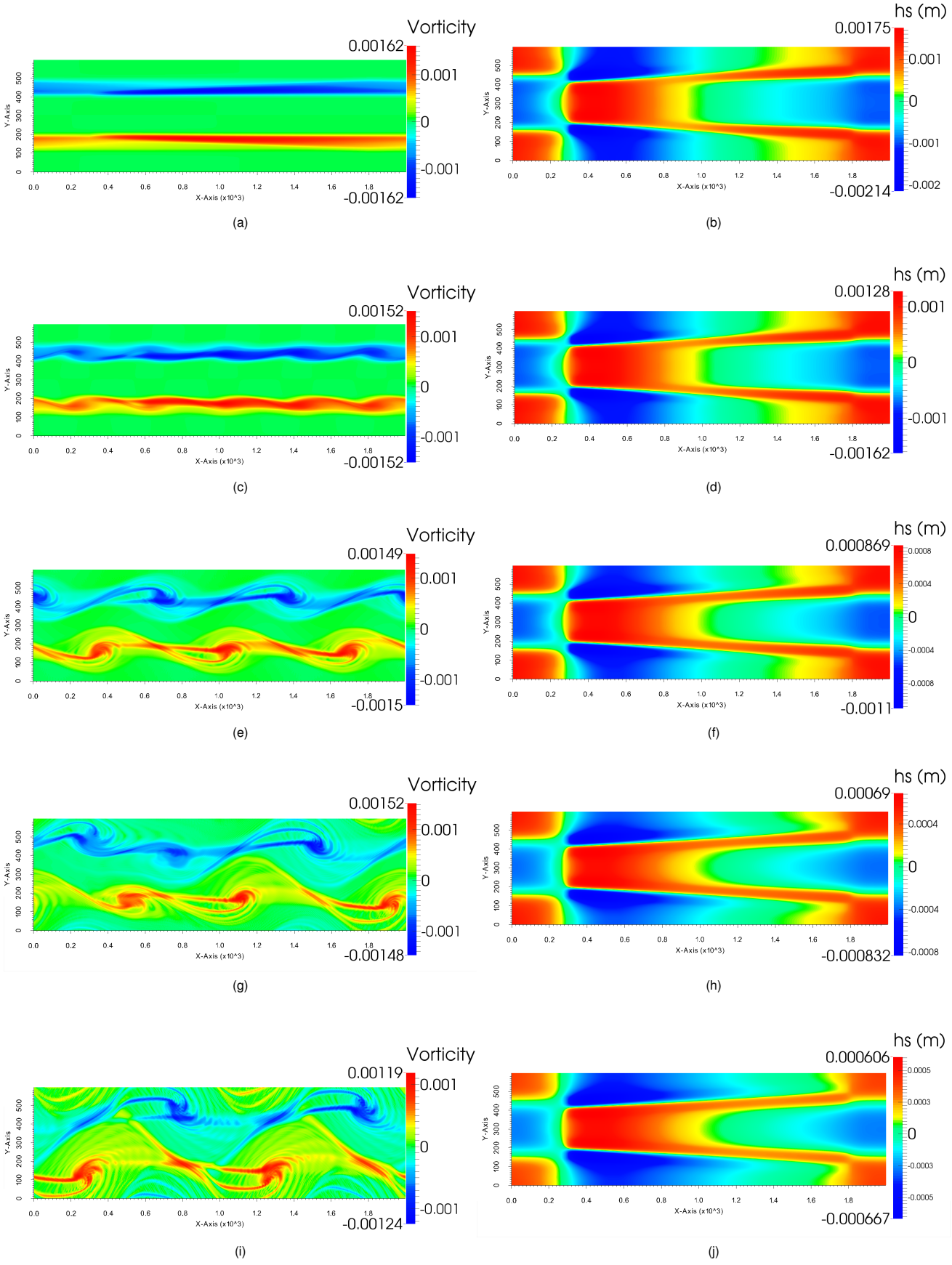

Figure 2: 2D vorticity (s^{-1}, left column) and seabed elevation (right column) fields after 11.5 days of dynamics. Cases H15 (a and b), H20 (c and d), H30 (e and f), H40 (g and h) and H50 (i and j).

4.1 Generation of instabilities and impact on morphological evolution

The results presented in figure 2 show that increasing water depth leads to the generation of instabilities in the wake. The ocean dynamics becomes turbulent, starting from a vortex formation at the wake boundaries. Furthermore, when eddies are generated, their size and spacing depend also on the water depth, as summarize in table 2.
For the different water depth studied here, three cases of ocean dynamics are observed. Up to 15 meters of water depth, the dynamics is laminar, the vorticity is higher at the wake boundaries than in other parts of the domain but no instabilities are generated (figure 2.a). When the water depth is between 20 and 30 meters, vortices are generated at all the wake boundaries (see figures 2.c and 2.e). Two independents localized vortex streets appear. The third case emerges when water depth is higher than 40 meters. As the size of the vortices increases, the two vortex streets interact leading to a domain wide turbulence (see figures 2.g and 2.i).
An increase of approximately a factor 2 of water depth leads to a change of the same order in the vortex spacing (Table 2). Decreasing the bottom friction coefficient in order to conserve the friction coefficient and water depth ratio ($S = C_D/h$) for two different water depth (cases H20CD2P3 and H30) gives similar results (figure 3.a and figure 3.b). It appears thus that vortex size and spacing seems to depend on S . This ratio, S, appears in the bottom friction terms in the SW equations:

$$\overrightarrow{G} = \frac{1}{h}\overrightarrow{\tau_b} = S \;||\; \overrightarrow{u} \;||\; \overrightarrow{u} \qquad [16]$$

This result confirms the findings of *Chen and Jirka* (1997) on the cylinder wake in a SW flow where $S = (D * C_D)/h$, with D the diameter of the cylinder. In the present paper no dependency test upon the wake width at the impact location (corresponding to the diameter of the cylinder of *Chen and Jirka* (1997) work) have been undertaken. Here, for increasing water depth, S is decreasing and the bottom friction force as well, allowing for stronger instabilities. For all the simulations undertaken, the qualitative spatial

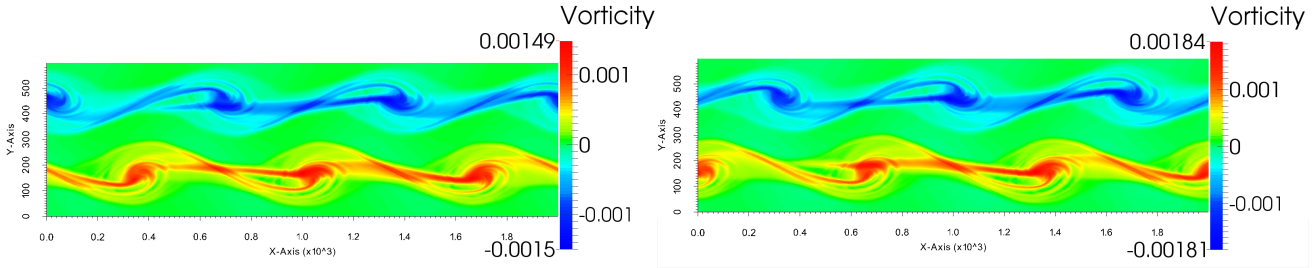

Figure 3: 2D vorticity seabed elevation fields after 11.5 days of dynamics. Cases H30 (a) and H20CD2P3 (b).

long-time impact on the wake upon the seabed is similar (figure 2, right column). Figure 2 shows that the velocity deficit induced by the wake leads to a sediment accumulation, $i.e$ a dune formation close to the impact (between $x = 300$m and $x = 500$m) which corresponds to the local wake width. The same phenomenon occurs at the wake boundaries. Such formations are due to the non uniformity of the oceanic velocity field and thus of the local bottom shear stress. Downstream in the wake, the velocity deficit becomes less important, corresponding to a bottom shear stress that induce bed erosion. Outside the wake, the flow velocity is higher, increasing thus the bottom shear stress and thus the sediment transport, leading to a hole formation on each side of the dune. After $x = 1000$m, the velocity and the bottom shear stress decrease along the x-direction, stopping the erosion and starting sediment accumulation when moving downstream in this region (figure 2, right column).

Figure 4 shows the bathymetry variation between two consecutive outputs ($\Delta t = 2000$ s) of the same simulation. The spatial pattern of the morphodynamical evolution between the turbulent and the laminar cases is completely different. The vortices strongly affect the short term seabed morphodynamics, as expected. For cases H15 and H20 (figures 4.a and 4.b, respectively), the bathymetry variations between two consecutive outputs are qualitatively similar to the seabed elevation fields after 11.5 days of dynamics. This is not the case from 30 m to 50 m water depth (figures 4.c and 4.d, respectively), the wakes imprint is totally annihilated by the signature of the large scale vortices. Difference in vortex scale observed in the ocean is recovered in the seabed, showing that vortex formation in the ocean has an significant impact on the seabed morphodynamics.
Considering the morphodynamical evolution, three cases can be observed, depending on whether the ocean dynamics is laminar, has a localized or a domain wide turbulent behavior. In the first case, changes in seabed elevation are around a few millimeters per month (figure 2.b). Results are similar for the localized turbulence case with small spatial variations (figure 2.d). For the domain wide turbulence case, instantaneous seabed changes are of the order of a few millimeters per month (figure 4.d), whereas the transport averaged over several days decreases to a few tenths of millimeter per month (figure 2.j). This behavior is easily explained by the oscillating local velocity which transports sediments back and forth. This result may cause environmental issues. Sediment motion induced by the turbulent state in the ocean could increase the local turbidity and perturb the photosynthesis in the water column even when the long term accumulated transport is small.

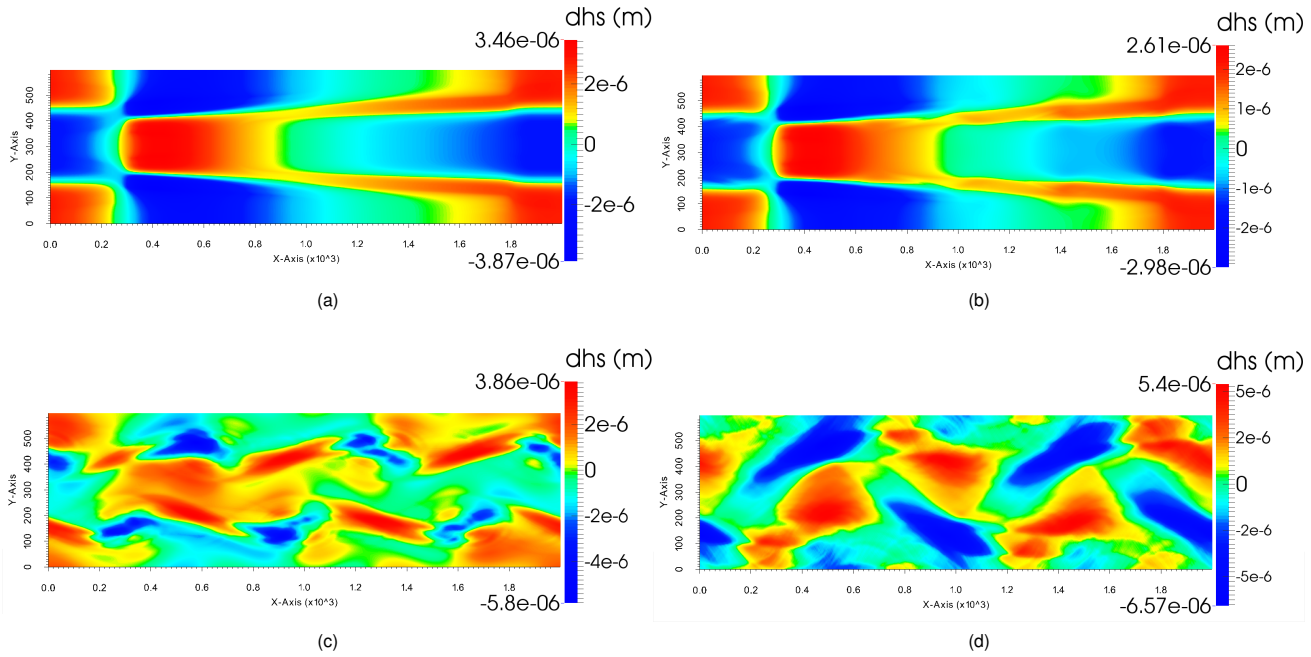

Figure 4: 2D bathymetry difference field between two consecutive outputs for H15 (a), H20 (b), H30 (c) and H50 (d) after 11.5 days.

4.2 Air-sea interactions and energetic balance

In this idealized model the source of mechanical energy is the atmospheric dynamics. Different computations have been undertaken using different water depth in order to quantify the energy transfer, the results are presented in figure 5. In this analysis, we neglected the y component of the velocity vectors, they are vanishing for the atmosphere and subdominant for the ocean.
The power lost by the atmosphere (P_a) is the integral over the domain of the product between the wind stress and the wind velocity.

$$P_\mathrm{a} = C_D \rho_a \int\int_S || \overrightarrow{u}_a - \overrightarrow{u}_o || \, (\overrightarrow{u_a} - \overrightarrow{u_o}) \cdot \overrightarrow{u_a} \, dS. \qquad [17]$$

As the y component of the velocity is vanishing in the atmosphere and subdominant in the ocean ($v_o \ll u_o, u_a$), equation (17) simplifies to:

$$P_\mathrm{a} = C_D \rho_a \int\int_S | \, u_a - u_o \, | \, (u_a - u_o) u_a \, dS. \qquad [18]$$

Furthermore, as the velocity in the atmosphere is always larger than in the ocean ($u_a > u_o, \ \forall x, \ \forall y, \ \forall t$):

$$P_\mathrm{a} = C_D \rho_a \int\int_S (u_a - u_o)^2 u_a \, dS. \qquad [19]$$

The power taken by the ocean (P_o) is the integral over the domain of the product between the wind stress and the ocean velocity, using the above simplifications it can be written as:

$$P_\mathrm{o} = C_D \rho_a \int\int_S (u_a - u_o)^2 u_o \, dS. \qquad [20]$$

According to the Betz theory, the maximal power value which can be taken from the wind by the turbine is lower or equal to 16/27 of the wind power without the turbine presence:

$$P_\mathrm{turbine} = \frac{16}{27} \left(\frac{1}{2} \rho_a \pi R^2 (u_a)^3 \right), \qquad [21]$$

where R correspond to the radius of the rotor.

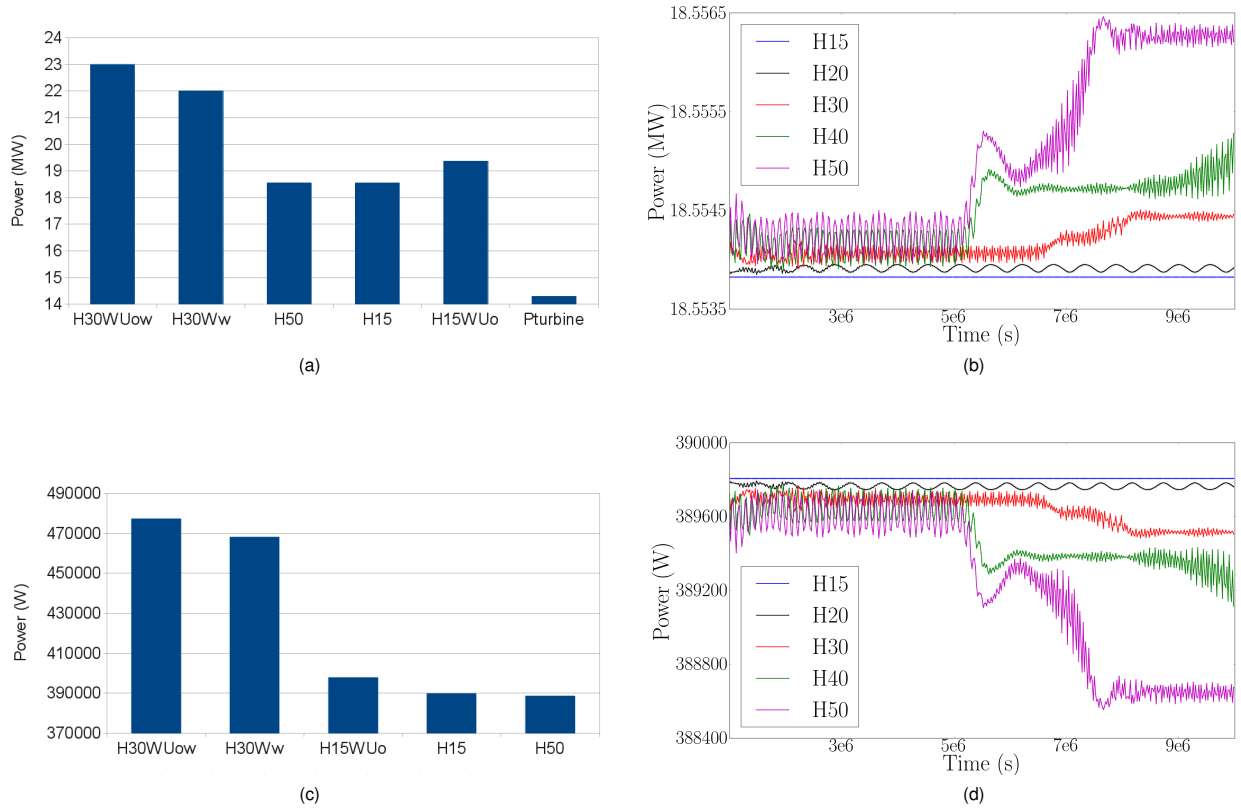

Figure 5: Power lost by the atmosphere for the different cases investigated and by the wind turbine (a), for different turbulent states (b) and power received by the ocean for the different cases investigated (c) and for different turbulent states (d).

Figure 5 shows that for all the cases investigated, the power received by the ocean from the atmosphere is several orders of magnitude lower than the power lost by the atmosphere (figures 5.a and 5.c). The major part of the power lost by the atmosphere is thus dissipated by the friction between the atmosphere and the ocean. Taking into account the ocean velocity in the wind forcing leads to a decrease by 2% of the power received by the ocean from the atmosphere (comparison between cases H30WUow, H30Ww and cases H15, H15WUo of figure 5.c) and by 4% of the power lost by the atmosphere (comparison between cases H30WUow H30Ww and cases H15, H15WUo of figure 5.a). For case H15, the loss of atmospheric power due to the friction is reduced by approximatively 4% as compared to case H15WUo. Taking into account the relative velocity between the atmosphere and the ocean leads to a reduction of the friction between these two layers and thus to the power loss by the atmosphere. Furthermore, considering the atmospheric wake presence leads to a decrease of the power received by the ocean and the one lost by the atmosphere of approximatively 16%. Such phenomenon may be explain by the fact that the wake impact reduces the local atmospheric velocity more than the local ocean one, the relative velocity between the two layers is thus decreasing, so as the friction.
For all the depths considered, the power loss to friction, which is the difference between the power lost by the atmosphere and the one received by the ocean, is higher than the power taken by the wind turbine.
The figures 5.b and 5.d show the power lost by the atmosphere and received by the ocean, respectively, for runs H15, H20, H30, H40 and H50. Values of the power lost are increasing for increasing water depth and thus increasing turbulence level (figure 5.b) but the values of power received by the ocean are decreasing for increasing water depths (figure 5.d). The difference between the values for the laminar (H15) and the domain wide turbulence case (H50) is small, of the order of 0.01% for the power lost by the atmosphere and of the order of 0.3% for the power received by the ocean. It shows that the oceanic turbulence as subdominant role in the air-sea energetic balance.

An analytical development can confirm and explain the above observations. Time average and developed equation 19 can be written for laminar and turbulent oceanic flow, respectively:

$$\overline{P_a{}^l} = C_D \rho_a \int\int_S {u_a}^3 - 2{u_a}^2 \overline{u_o} + u_a \overline{{u_o}^2}\, dS. \qquad [22]$$

$$\overline{P_a{}^t} = C_D \rho_a \int\int_S \underbrace{{u_a}^3}_{a_1} \underbrace{-2{u_a}^2 \overline{u_o} + u_a \overline{{u_o}^2}}_{a_2} + \underbrace{u_a \overline{{u_o'}^2}}_{a_3}\, dS, \qquad [23]$$

where $\overline{u_o}$ is the mean flow velocity and $\overline{u_o'^2}$ is the square of the velocity fluctuations, or the $x-$normal component of the Reynolds stress tensor.
The same procedure can be applied to the power received by the ocean (20) and gives for laminar and turbulent oceanic flow, respectively:

$$\overline{P_o{}^l} = C_D \rho_a \int\int_S {u_a}^2 \overline{u_o} - 2u_a \overline{u_o{}^2} + \overline{u_o{}^3}\, dS. \quad [24]$$

$$\overline{P_o{}^t} = C_D \rho_a \int\int_S \underbrace{{u_a}^2 \overline{u_o}}_{o_1} \underbrace{-2u_a \overline{u_o{}^2} + \overline{u_o{}^3}}_{o_2} + \underbrace{\overline{u_o'^2}(3\overline{u_o} - 2u_a)}_{o_3}\, dS. \quad [25]$$

The importance of the different terms in the air-sea energetic balance appears in the equations (22), (23), (24) and (25). The terms $a_1 = {u_a}^3$ and $o_1 = {u_a}^2 \overline{u_o}$ are linked to the power taken by the ocean without taking into account the oceanic velocity in the atmospheric forcing. These terms are predominant in laminar and turbulent equations. The terms $a_2 = -2{u_a}^2 \overline{u_o{}^2} + u_a \overline{u_o{}^2}$ and $o_2 = -2u_a \overline{u_o{}^2} + \overline{u_o{}^3}$ correspond to mean flow power correction occurring when the oceanic velocity is taking into account in the atmospheric forcing. As the velocity in the atmosphere is always much larger than in the ocean, these correction terms are negative. Taking into account the oceanic velocity in the atmospheric forcing leads thus to reduce both P_a and P_o.
For equations (23) and (25) the terms $a_3 = u_a \overline{u_o'^2}$ and $o_3 = \overline{u_o'^2}(3\overline{u_o} - 2u_a)$ correspond to the contributions of the turbulent fluctuations in the energetic balance. The terms $a_3 > 0$ and $o_3 < 0$, at least for the idealized situation considered here. When turbulence occurs in the domain, it increases thus the power lost by the atmosphere but decreases the power received by the ocean, a result in agreement with the observations done in figures 5.b and 5.d. This can be explain by the fact that a part of the turbulent fluctuations is not in the same direction as the oceanic motion and the atmospheric forcing and increases thus the friction between the two layers. Furthermore, these fluctuations certainly reduce the energetic transfer efficiency to the mean flow which may explain that they decrease the power received by the ocean.

If the turbulence seems to play a minor role in the air-sea energetic balance, the results presented in Section 4.1 show its importance on both oceanic and morphological dynamics. The equations (23) and (25) seem to show that evaluating the $x-$component of the root$-$mean$-$square velocity ($U_{\mathrm{rms}} = \sqrt{\overline{u_o'^2}}$) of the fluctuations can be used to estimate the importance of turbulent fluctuations in the ocean for the energy fluxes at the atmosphere-ocean interface.

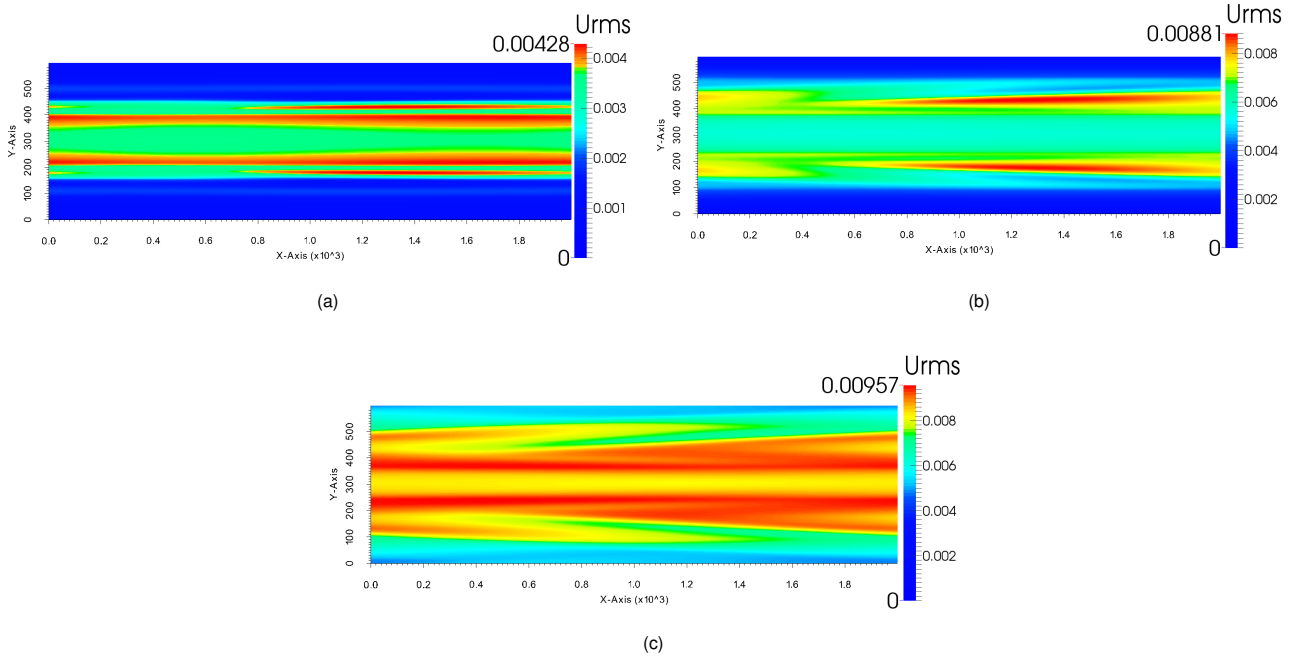

Figure 6: 2D U_{rms} fields for H20 (a), H20CD2P3 (b) and H50 (c) after 11.5 days of dynamics.

Figure 6 shows the 2D U_{rms} fields for different cases investigated. For each case, the maximum of U_{rms} is localized at the wake boundaries, where eddies are generated. This is particularly clear for case H20 and H20CD2P3 (figures 6.a and 6.b, respectively) where the vortex streets are independent. When the turbulence is domain wide (figure 6.c), the highvalues of U_{rms} are less localized and start to fill large parts of the domaine. Furthermore, the maximum value of the U_{rms} is increasing for increasing water depth. The maximum value of the U_{rms} is equal to 0.00957 m.s^{-1} (for the H50 case), which is only 2.4% of the mean velocity (of the order of 0,4 m.s^{-1}), showing once again the fluctuation's small order of magnitude compared to the mean flow.

Computations of the $V_{\rm rms} = \sqrt{\overline{v_o'^2}}$ velocity (figure 7) show that the $y-$component of the turbulent fluctuations is of the same order of magnitude than the x ones.

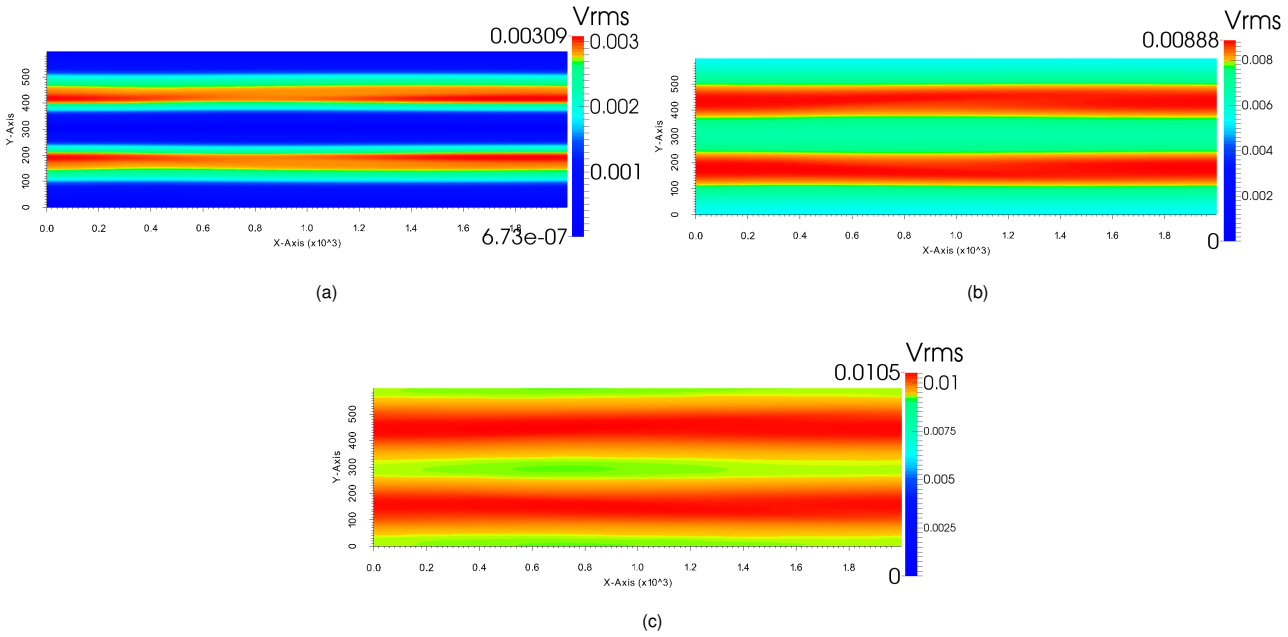

Figure 7: 2D $V_{\rm rms}$ fields for H20 (a), H20CD2P3 (b) and H50 (c) after 11.5 days of dynamics.

Variations of free surface elevation for the different computations undertaken are extremely small, of the order of thenths of a millimeter. The dynamic height is thus small, a result in agreement with potential energy calculations showing that potential energy involved in the problem is eight orders of magnitude lower than kinetic energy. The major part of the energy involved in the problem is thus kinetic and not potential.

5. SUMMARY AND CONCLUSION

An idealized 2D numerical model has been proposed to study the impact of an offshore wind turbine wake on the ocean and sediment dynamics. To the best of our knowledges so far no study has been done on this subject.
A simplified physical model has been proposed and a mathematical model has been consistently built.

The present results show that the turbine wake has an impact on both ocean and sediment bed layers. Turbine wake impact on the ocean surface can generate instabilities and vortex streets formation. Size and spacing between these vortices seems to be controlled by the friction between the bed and the ocean layer and more precisely by the friction coefficient and water depth ratio, $S = C_D/h$. When S is decreased, large scale instabilities are more easily generated, leading to a domain wide turbulence state in the ocean.
Concerning the seabed, results show that the non-uniformity of the oceanic velocity field induced by the wake presence is recovered in the local bottom shear stress responsible for sand erosion and deposition. As the vortices strongly affect the seabed morphodynamics, for localized and domain wide turbulence, the wakes imprint tends to be reduced by large scale vortices and the oscillating local velocity which transports sediments back and forth.
Taking into account the ocean velocity in the wind forcing leads to a decrease by approximatively 4% of the power loss to friction of the atmosphere, for the case considered here, by reducing the relative velocity between the two layers. Power received by the ocean is also decreasing by approximatively 2%. Finally, considering the wake presence leads to a decrease of 16% of the power received by the ocean, as the local air-sea friction is decreased.
The results also show that even if the turbulence is strongly influencing both, oceanic and morphological dynamics its role is minor in the air-sea energetic balance. Furthermore, as the atmospheric dynamics is not resolved here, the oceanic turbulence has a limited retro-action on the forcing, considering the atmosphere as a shallow-water layer may increase the importance of these interactions.

Acknowledgements We thank Cyrille Bonamy for the parallelization of the code and for his precious help in the numerical implementation and the Institut Carnot Énergies du Futur for their financial support. All the computations presented in this paper were performed using the Froggy platform of the CIMENT infrastructure (https://ciment.ujf-grenoble.fr), which is supported by the Rhône-Alpes region (GRANT CPER07-13 CIRA) and the Equip@Meso project (reference ANR-10-EQPX-29-01) of the programme

Investissements d'Avenir supervised by the Agence Nationale pour la Recherche.

REFERENCES

Barbe, J. B. (2013), *Etude de l'impact des éoliennes offshores sur l'ocean et l'atmosphere - Internship report*.

Breusers, H., and A. Raudkivi (1991), *Scouring*, Balkema Rotterdam.

Breusers, H., G. Nicollet, and H. Shen (1977), Local scour around cylindrical piers, *Journal of Hydraulic Research*, *15*(3), 211–252.

Chen, D., and G. H. Jirka (1997), Absolute and convective instabilities of plane turbulent wakes in a shallow water layer, *Journal of Fluid Mechanics*, *338*, 157–172.

Drewitt, A. L., and R. H. Langston (2006), Assessing the impacts of wind farms on birds, *Ibis*, *148*(s1), 29–42.

EWEA (2013), *Deep water, the next step for offshore wind energy*.

Jacobson, M. Z., C. L. Archer, and W. Kempton (2014), Taming hurricanes with arrays of offshore wind turbines, *Nature Climate Change*, *4*(3), 195–200.

Jensen, N. (1983), *A note on wind generator interaction*, Risø-M-2411, Risø National Laboratory.

Jiang, G.-S., D. Levy, C.-T. Lin, S. Osher, and E. Tadmor (1998), High-resolution nonoscillatory central schemes with nonstaggered grids for hyperbolic conservation laws, *SIAM Journal on Numerical Analysis*, *35*(6), 2147–2168.

Meyer-Peter, E., and R. Müller (1948), Formula for the bedload transport, in *3rd Meeting of the International Association of Hydraulic Research*.

Moulin, A., and A. Wirth (2014), A drag-induced barotropic instability in air–sea interaction, *Journal of Physical Oceanography*, *44*(2), 733–741.

Roulund, A., B. Sumer, J. Fredsøe, and J. Michelsen (2005), Numerical and experimental investigation of flow and scour around a circular pile, *Journal of Fluid Mechanics*, *534*, 351–401.

Shields, A. (1936), Anwendung der ahnlichkeits mechanik und der turbulenzforschung auf die geschiebebewegung, in *Mitteilungen der Preußischen Versuchsanstalt für Wasserbau, Berlin*.

Smith, S. (1988), Coefficients for sea surface wind stress, heat flux, and wind profiles as a function of wind speed and temperature, *Journal of Geophysical Research: Oceans (1978–2012)*, *93*(C12), 15,467–15,472.

Tucker, V. (1996), A mathematical model of bird collisions with wind turbine rotors, *Transactions-American Society of Mechanical Engineers Journal of Solar Energy Engineering*, *118*, 253–262.

Van der Veen, H. H., S. Hulscher, and B. Perez Lapena (2007), Seabed morphodynamics due to offshore wind farms, in *River, Coastal and Estuarine Morphodynamics: RCEM*.

Vautard, R., F. Thais, I. Tobin, F.-M. Bréon, J.-G. Devezeaux de Lavergne, A. Colette, P. Yiou, and P. M. Ruti (2014), Regional climate model simulations indicate limited climatic impacts by operational and planned european wind farms, *Nature communications*, *5*.

Wu, J. (1982), Wind-stress coefficients over sea surface from breeze to hurricane, *Journal of Geophysical Research: Oceans (1978–2012)*, *87*(C12), 9704–9706.